A Connection Between Star Formation Rate and Dark Matter Halos at $Z \sim 6$ In 2013 Planck Cosmology.

F.L. Gómez-Cortés[1]

Departamento de Fsica, Universidad de los Andes, Colombia

Received _____; accepted _____

ABSTRACT

This work relates baryonic matter and dark matter at redshift $z = 5.9$ using observational data from CFHTLS (Willott et al. 2013), HST Legacy Survey (Bouwens et al. 2014; Finkelstein et al. 2014), UKIDSS and SDXS (McLure et al. 2009), and results of the Multidark Simulation (Riebe 2013) in a cubic box of 1000Mpc h^{-1} length with 2013 Planck Cosmology. The Luminosity Function (LF) is fitted via four parameters with the Markov Chain Monte Carlo method. The relationship between the Dark Matter Halos Mass and Star Formation Rate is obtained using the relationship between the UV continuum (from the fitted LF) and Star Formation Rate (SFR) by Kennicutt (1998).Cosmic variance effects are studied on smaller boxes of 250Mpc h^{-1} length.

Halos.

Subject headings: Dark Matter, LF, SFR, High Redshift Galaxies, Reionization

0.1. The Luminosity Model

In this model we have made two assumptions:

1. Each halo in the catalog hosts one galaxy. There are not empty halos, also none of halos has two or more galaxies.

2. The UV luminosity of each galaxy is function of one variable: the mass of the DMH in wich is located.

The simplest relation we can have is a powerlaw:

$$L = L_0 M^{\alpha} \tag{1}$$

but has not well agreement with observed luminosity functions.

A better model is a four parameter function. Each galaxy has a luminosity given by:

$$L = L_0 M \left[\left(\frac{M}{M_0} \right)^{-\beta} + \left(\frac{M}{M_0} \right)^{\gamma} \right]^{-1} \tag{2}$$

where M is the hosting DMH mass, L_0 is a normalization constant, M_0 is the critical mass where the luminosity function has a slope change, β and γ are the slopes. This equation has a similar fashion to the mass to light relation (van den Bosch 203) and the mean relation between stellar mas of a galaxy and the mas of its halo used by Moster (2010).

There are more complex models(Lee 2009) that includes a random behavior: galaxies has not synchronization on the beginning of star forming stage, also this stage may be time limited. This is called duty cycle. It is probable to have in the observations some invisible galaxies in the UV continuum due their duty cycle may has not started as well it may ended. Also may be present a normal distribution of the luminosity around the expected values.

0.2. Star Formation Rate

The age of a star can be estimated by analyzing its spectrum. But when far galaxies are studied, individual stars can not be resolved. Is not possible to make a detailed census of the galaxy popullation. Only is possible to get information from the whole stellar population, an integrated spectrum.

There is a method(Madau 1998) in wich a linear relation between SFR and luminosity in specific wavelength ranges can be assumed. This model allows to estimate the young stars fraction and the mean SFR over periods of $10^8 - 10^9$yr(Kennicutt 1998). The luminosity in the model, comes from the UV and the FIR broadband, also from speciffic recombination lines.

In a typical galaxy spectrum the visible wavelengths are dominated by the main sequence stars (A to early F) and G-K giants. In few wavelength ranges we have a significative contribution from the young stars rather than the old stars. The infrared and far infrared wavelengths emission is dominated by dust, this dust is heated by the whole stellar popullation, in particular by young, UV-bright stars (Law 2011).

On active galaxies the UV broadband emission is dominated by late-O and early-B type stars, with temperature near to 40.000K. These hot and massive stars has a lifetime below 10^7Gyr, they spend their nuclear fuel faster than smaller and cooler sunlike stars.

The relation between UV luminosity and Star Formation Rate (Madau 1998; Kennicutt 1998) is given by:

$$\mathrm{SFR}\left(M_\odot \mathrm{yr}^{-1}\right) = 1.4 \times 10^{-28} L_\nu \left(\mathrm{erg\ s}^{-1}\mathrm{Hz}^{-1}\right) \tag{3}$$

With Initial Mass Function (IMF) between $0.1M_\odot$ and $100M_\odot$, in the range of $1250 - 2500$Å

The star forming rate will be:

$$SFR = k \times L_0 M \left[\left(\frac{M}{M_0} \right)^{-\beta} + \left(\frac{M}{M_0} \right)^{\gamma} \right]^{-1} \tag{4}$$

0.3. Dust Absorption

1. Observations

This paper is based on four main observational data sets from the Hubble Space Telescope and three ground-based telescopes. All $z \sim 6$ LBG candidates where discovered using using the drop-out technique(Steidel 2003). All magnitudes are in AB system.

The data from the Hubble Space Telescope Legacy (HSTL) (Bouwens et al. 2014) is a compilation of observations since the installation of the Advanced Camera for Surveys (ACS) in 2002, through the near-infrared Wide Field Camera 3 (WFC3/IR) installed in 2009, up to 2012. The HST fields of view are: XDF, HUDF09-1, HUDF09-2, CANDELS-S/Deep, CANDELS-S/Wide, ERS, CANDELS-N/Deep, CANDELS-N/Wide, CANDELS-UDS, CANDELS-COSMOS and CANDELS-EGS, with areas of 4.7, 4.7, 4.7, 64.5, 34.2, 40.5, 62.9, 60.9, 151.2, 151.9 and 150.7 arcmin^2 respectively. The total area corresponds to $\sim 0.7\,\mathrm{deg}^2$ over five different lines of sight, reducing cosmic variance effects. Two cameras performed the observations: ACS and WFC3/IR, using B_{435}, V_{606}, i_{814}, z_{850}, I_{814}, Y_{098}, Y_{105}, $J125$, JH_{140} and H_{160} filters. The limit magnitude is between $\sim$ 27.5mag in CANDELS-EGS and$\sim$ 30mag in the deepest field (XDF). Total number of z=6 LBG candidates is 940, most of them in the faint end of the LF, magnitudes in the rest frame are in the range $-22.52 \leq M_{1600} \leq -16.77$ **?** calculated LF using a stepwise maximum-likelihood (SWML) based on Efstathiou et al. (1988). The Schechter parameters derived are: $\phi^*/\mathrm{Mpc}^{-3} = (0.33^{+0.15}_{-0.10}) \times 10^{-3}$, $M^*_{1600} = -21.16 \pm 0.20$ and $\alpha = -1.91 \pm 0.09$. Bouwens et al. (2014) reported that using just few fields of view, UVLF has a slightly non-Schechter-like form.

Finkelstein et al. (2014) worked also with HST, using the HUDF, CANDELS and GOODS fields, along with two of the Hubble Frontier Fields (HFF): deep parallel observations (unlensed fields) near the Abell 2744 and MACS J0416.1-2403 clusters. The HFF uses the ACS and the WFC3/IR with the same filters aforementioned but z_{850}.

Willott et al. (2013) presented the sixth release of the Canada-France-Hawaii Telescope Legacy Survey CFHTLS. The observations where performed over four separated fields covering a total area $\sim 4\,\mathrm{deg}^2$ (a large area), it gives this survey great robustness. Optical observations used MegaCam with $u^*g'r'i'z'$ filters. The main selection criteria: all the objects must be brighter than magnitude $z' = 25.3$. The final number of LBGs founded was 40. Moreover, they get spectroscopic confirmation for 7 candidates using GMOS spectrograph on the Gemini Telescopes, which has a $\ll 5.5$-square arcmin field of view . They show incompleteness in the sample due to foreground contamination and the detection algorithm; there is no warranty to have every object brighter than the limit magnitude on the faint limit. The full galaxy LF at $z = 6$ cannot be obtained as in other studies. Nevertheless, this survey was focussed on the highly luminous LBGs. LF is calculated using the stepwise maximum likelihood method of Efstathiou et al. (1988), within magnitudes from $M_{1350} = -22.5$ up to -20.5. The luminosity function of $z = 5.9$ shows an exponential decline at the bright end, where feedback processes and inefficient last cooling limites star forming in bright galaxies hosted in the most massive halos.

McLure et al. (2009) build the luminosity function for $z = 5$ and $z = 6$ using data from two ground-based telescopes: the United Kingdom Infrared Telescope in the near-IR imaging and Subaru Telescope for the optical imaging. They use the first data release of the UKIRT Infrared DeepSky Survey Ultra Deep Survey (UDS), together with the Subaru XMM-Newton Survey (SXDS). Total observed area is $0.63\,\mathrm{deg}^2$ uniformly covered by booth catalogues. The UKIRT was equipped with the WFCAM using JK filters. The Subaru was equipped with the Suprime-Cam with the $BVRi'z'$ filters. All candidates where brighter than $z' = 26$. The UV rest frame magnitude range is $-22.4 \leq M_{1500} \leq -20.6$. The LF was calculated using the maximum likelihood estimator of Schmidt (1968). Their analysis gave a total number of 104 LBG candidates in the redshift range $5.7 \leq z \leq 6.3$. LF was parameterized according to the Schechter function with $\phi^*/\mathrm{Mpc}^{-3} = (1.8 \pm 0.5) \times 10^{-3}$,

$M^*_{1500} = -20.04 \pm 0.12$ and $\alpha = -1.71 \pm 0.11$.

The dataset was retrieved from McLure et al. (2009) graph using GAVO-DEXTER[1].

[1]http://dc.zah.uni-heidelberg.de/dexter/ui/ui/custom

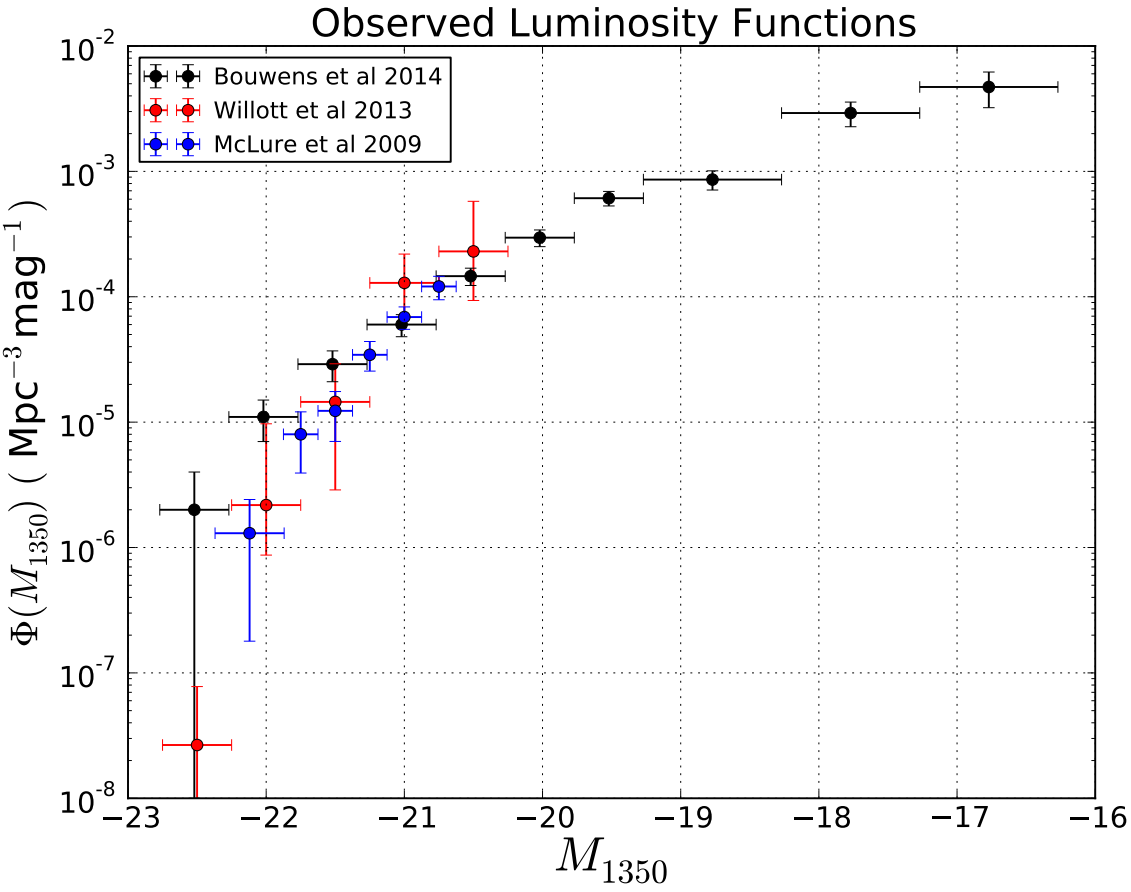

Fig. 1.— Observational data from Bouwens et al. (2014); McLure et al. (2009)and Willott et al. (2013).

2. Methodology

The first goal in this paper is reproduce the observed UVLF from DMH, from simulations at redshift $z = 6$. The observational datasets where aforementioned.

Bolshoi Simulation (Riebe 2013) was performed by the MuldiDark consortium MultiDark Database is

UV Luminosity as function of DMH mass. Parameters. Dust Extinction

MCMC, maximum likelihood.

UV luminosity to SFR

3. Discussion

(Lundgren 2014(@) SFR evolution from $z = 1$ to 6

(Bouwens et al. 2014) HST Legacy

(Jiang 2011) Keck pectroscopy

"Fig. 16. Updated Determinations of the derived SFR (left axis) and U V luminosity (right axis) densities versus redshift (5.4). The left axis gives the SFR densities we would infer from the measured luminosity densities, assuming the Madau et al. (1998) conversion factor relevant for star-forming galaxies with ages of 108 yr (see also Kennicutt 1998). The right axis gives the U V luminosities we infer integrating the present and published LFs to a faint-end limit of 17 mag (0.03 L)"BOUWENS 2014 UV LF

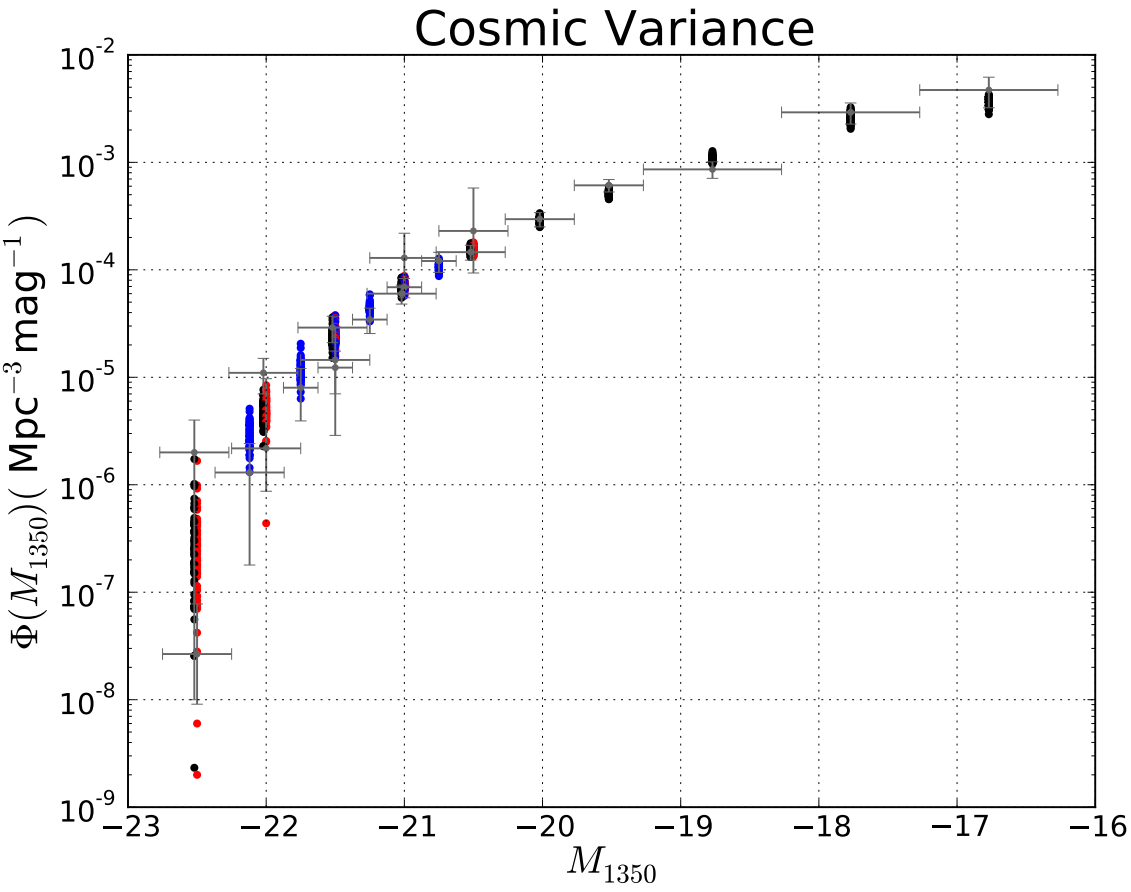

Fig. 2.— Cosmic Variance: The Luminosity Function is made using the DMH catalog from the full box and the set of parameters from the small boxes.

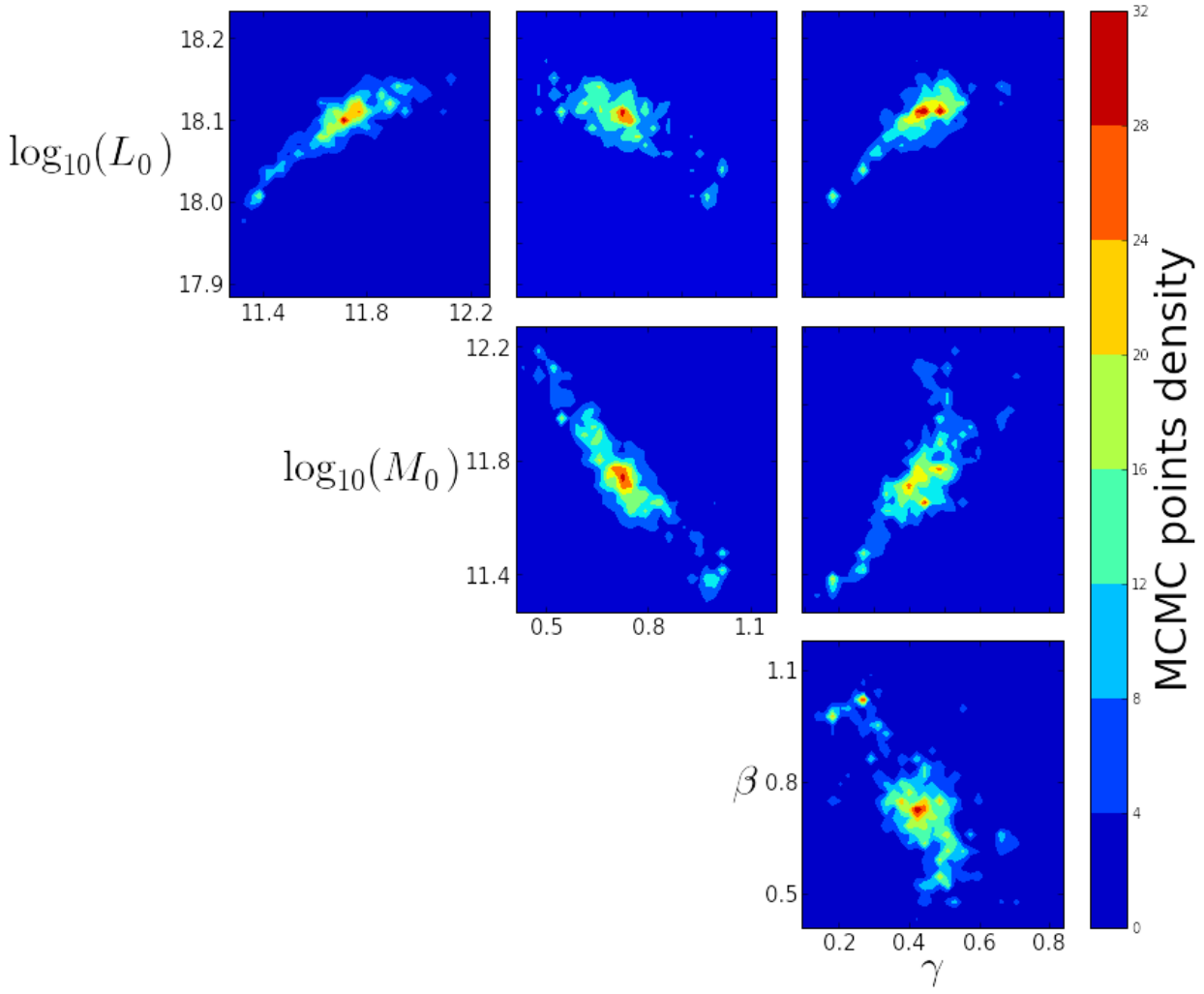

Fig. 3.— Covariance of parameters for one small box

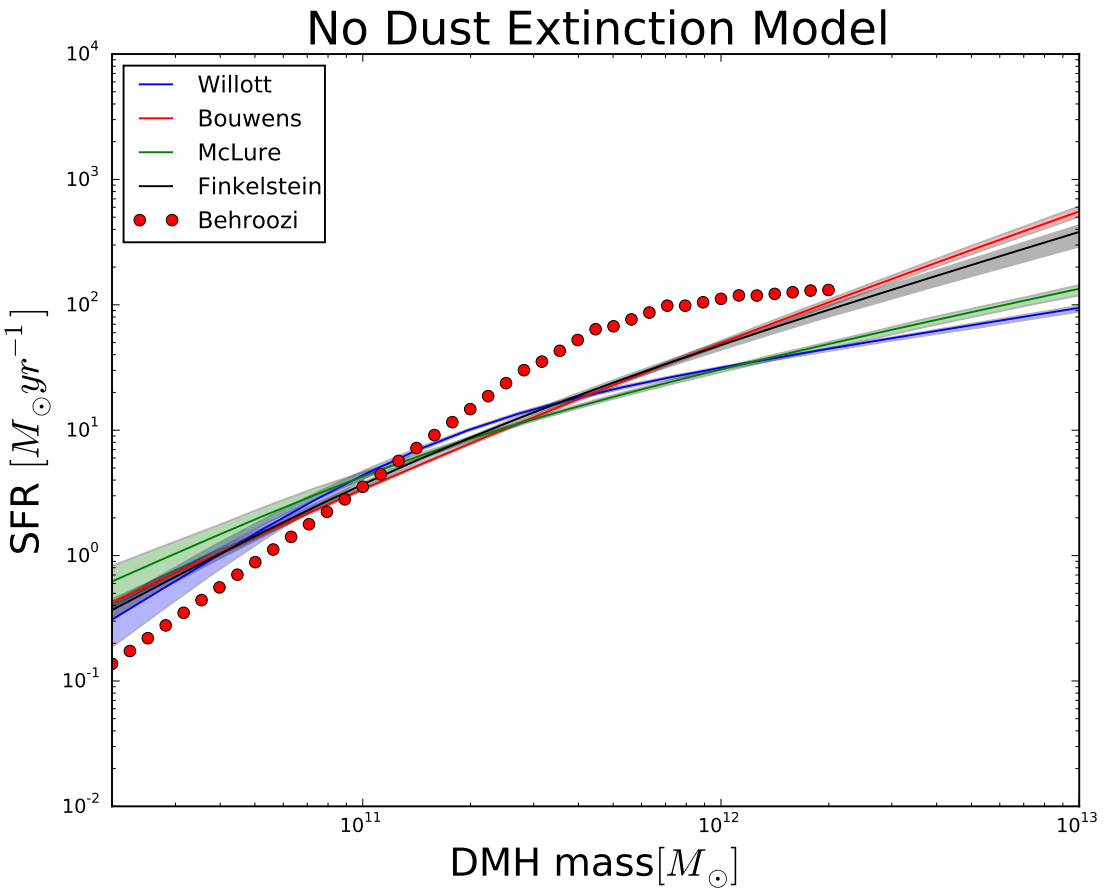

Fig. 4.— Star formation rate as function of the dark matter halo mass without dust attenuation. Solid lines represents the mean SFR value over the small boxes within 50% shaded region.

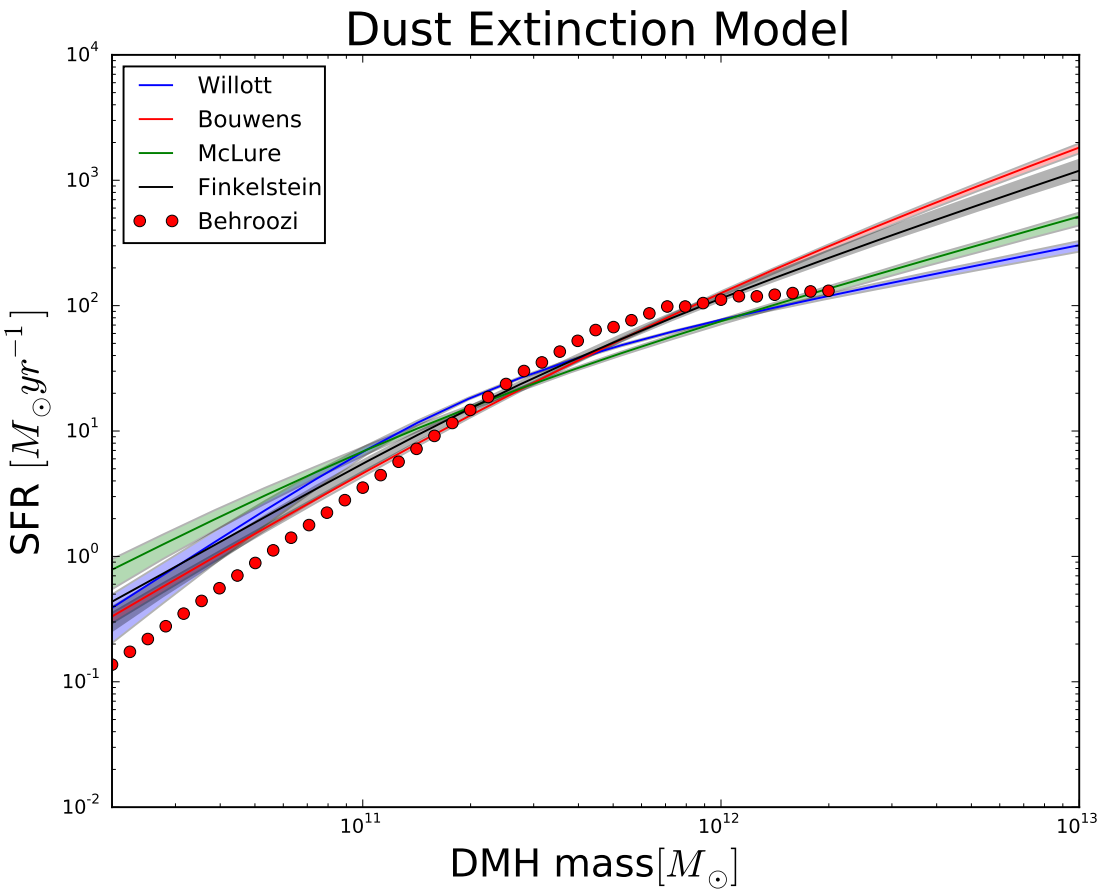

Fig. 5.— Star formation rate as function of the dark matter halo mass with dust attenuation. Solid lines represents the mean SFR value over the small boxes within 50% shaded region.

4. Summary

REFERENCES

Bouwens, R. J. et al. 2006, ApJ, 653, 53

Bouwens, R. J. et al. 2012, ApJ, 752, 5

Bouwens, R. J., G. D. Illingworth, P. A. Oesch, M. Trenti, I. Labbe', L. Bradley, M. Carollo, et al. 2014, arXiv:1403.4295

Efstathiou, G., Richard S. Ellis, and Bruce A. Peterson. 1988, MNRAS, 232,431.

Finkelstein, Steven L., Russell E. Ryan Jr., Casey Papovich, Mark Dickinson, Mimi Song, Rachel Somerville, Henry C. Ferguson, et al. 2014, arXiv:1410.5439

Kennicutt, Robert C., Jr. 1998, ARA&A, 36, 189

Kennicutt, Robert C., Jr et al. 2009, ApJ, 703, 4672

Law, K. et al. 2011, ApJ, 738, 124

Jiang, Linhua et al. 2011, ApJ, 743, 65

Lee, Kyoung-Soo et al. 2009, ApJ, 695, 368

Lundgren, Britt F. et al, 2014, ApJ, 780, 34

Madau, Piero. et al, 1998, ApJ, 498, 106M

McLure, R. J., M. Cirasuolo, J. S. Dunlop, S. Foucaud, O. Almaini. 2009, MNRAS, 395, 2196

Moster, Benjamin P. et al. 2010, ApJ, 710, 903

Riebe, K. et al. 2013, AN, 334, 691

Schmidt, Maarten. 1968, ApJ151, 393.

Steidel, Charles C. et al. 2003, ApJ, 592, 728

Trible, Virginia. 1987, ARA&A, 25, 425

van den Bosh, Frank C. et al. 2003, MNRAS, 40, 771

Willott, Chris J., Ross J. McLure, Pascale Hibon, Richard Bielby, Henry J. McCracken, Jean-Paul Kneib, Olivier Ilbert, David G. Bonfield, Victoria A. Bruce, Matt J. Jarvis. 2013, AJ, 145, 4